A generalized model for conic flexure hinges

Guimin Chen, Xiaoyuan Liu, Hongwei Gao, and Jianyuan Jia
School of Mechatronics, Xidian University, Xi'an, Shaanxi 710071, People's Republic of China

(Received 25 December 2008; accepted 27 April 2009; published online 19 May 2009)

Flexure hinges have been used to produce frictionless and backlashless transmission in a variety of precision instruments. Many kinds of flexure profile were proposed during the past decade. The present work brings elliptical arc, parabolic, and hyperbolic profiles together by proposing a generalized conic flexure hinge model. By utilizing the generalized equation for conic curves in polar coordinates, all the elements in the compliance and precision matrices for conic flexure hinges are deduced. These equations were verified by finite element analysis and experimentation. The analytical results are within 11% error compared to the finite element results and within 6% error compared to the experimental results. © *2009 American Institute of Physics.*
[DOI: 10.1063/1.3137074]

I. INTRODUCTION

Flexure hinges have been used to produce frictionless and backlashless transmission in a variety of precision instruments such as micro- and nanomanipulating platforms, high-accuracy alignment devices, and displacement amplifiers for piezoelectric actuators. The performance of flexure-based mechanisms is highly dependent on the characteristics of flexure hinges; therefore, the design of flexure hinges is of practical importance.

In the previous work on this subject, flexure hinges of various cutout profiles have been introduced and discussed. Paros and Weisbord[1] proposed circular flexure hinges and derived both full theoretical and simplified design equations for them. Smith *et al.*[2] presented elliptical flexure hinges and their compliance equations. Chen *et al.*[3] extended the definition of elliptical hinges by changing the maximum eccentric angle ϕ_m of the cutout profiles from $\phi_m=\pi/2$ (semiellipse) to $0<\phi_m\leq\pi/2$ and correspondingly called them elliptical arc flexure hinges. The closed-form compliance equations were derived for elliptical arc flexure hinges using the Cartesian coordinates, which can also be used to design circular, right-circular, and elliptical flexure hinges. Lobontiu *et al.*[4] introduced two new configurations, namely, parabolic and hyperbolic flexure hinges, and developed their analytical equations, respectively. The Computerized Numerical Controlled (CNC) machining technology, especially the Wire electrical discharge machining (WEDM), enables high-precision and low-cost fabrication of flexure hinges of arbitrary cutout profiles. However, circular flexure hinges are often used because it is burdensome for a designer to work with all these types of flexure hinges and their corresponding design equations in order to find the optimal profile.

There are two chief aspects to consider when designing flexure hinges for a flexure-based mechanism, namely, the cutout profile selection and the parameter design of flexure hinges. Because the two aspects are theoretically independent, and there are no clear-cut guidelines for selection of the cutout profile, flexure hinge design is always performed first by selecting a certain type of flexure hinge (based on the designer's experience) and then designing the parameters using the corresponding design equations.[5–7] This situation prohibits designers from confidently and consistently finding the most suitable hinge designs (since accounting for all cutout profiles would prove very burdensome and choosing only one necessarily excludes others which may be better). In this work, we propose a solution to this problem in the form of a generalized flexure hinge model with one set of design equations which includes multiple types of conic flexure hinges, effectively combining the aspects of cutout profile selection and parameter design into one.

By basing our proposal on the general form of conic equations in polar coordinates, we are able to propose a generalized model for conic flexure hinges which encompasses elliptical arc, parabolic, and hyperbolic flexure hinges. Figure 1 shows the three-dimensional geometry of a conic flexure hinge. The geometric parameters include the minimum thickness t, the cutout length $l=2a$, the cutout depth c, and the cross-sectional width w. The generalized closed-form equations, including the compliance equations and precision equations, are derived for conic flexure hinges using polar coordinates. These generalized equations allow users to select cutout profiles and design parameters simultaneously, drastically improving the chances of selecting the most suitable hinge for the application. It should also be noted that this work extends the definition of hyperbolic flexure hinges given by Lobontiu *et al.*,[4] which will be discussed in detail in Sec. III C.

II. THE GENERALIZED EQUATION FOR CONIC CURVES IN POLAR COORDINATES

Figure 2 shows a conic curve along with its directrix and focus F. In polar coordinates, the conic curve with focus F on the pole can be expressed as

$$r(\theta)=\frac{ep}{1+e\cos\theta}, \tag{1}$$

where $p(p>0)$ is the distance between the focus and the corresponding directrix, and $e(e>0)$ is the eccentricity, which is determined by

 © 2009 American Institute of Physics

Author complimentary copy. Redistribution subject to AIP license or copyright, see http://rsi.aip.org/rsi/copyright.jsp

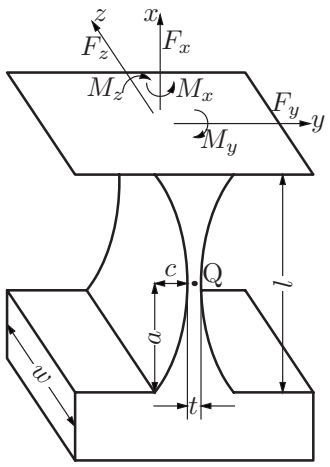

FIG. 1. Schematic of a conic flexure hinge.

$$e = \frac{r(\theta)}{m(\theta)}. \tag{2}$$

If $0<e<1$, the conic is an ellipse, if $e=1$, the conic is a parabola, and if $e>1$, it is a hyperbola. Assuming the conic cutouts of conic flexure hinges start from $-\theta_m$ and end at θ_m (θ_m is called the maximum polar angle, as shown in Figs. 3–5. In this generalized model for conic hinges, e, p, and θ_m are design parameters for the hinge cutouts), the cutout length can be calculated as

$$l = 2a = 2r(\theta_m)\sin\,\theta_m = \frac{2ep\,\sin\,\theta_m}{1+e\,\cos\,\theta_m} \tag{3}$$

and the cutout depth as

$$c = -\,r(\theta_m)\cos\,\theta_m + \frac{ep}{1+e} = -\,\frac{ep\,\cos\,\theta_m}{1+e\,\cos\,\theta_m} + \frac{ep}{1+e}. \tag{4}$$

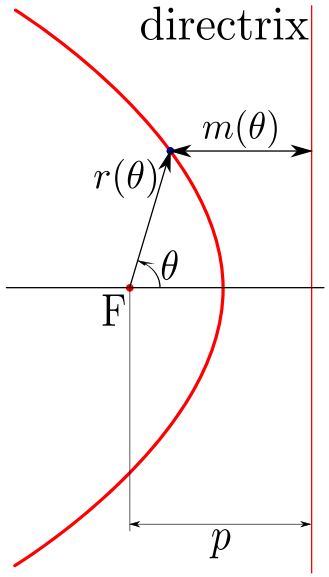

FIG. 2. (Color online) A conic and its polar coordinates.

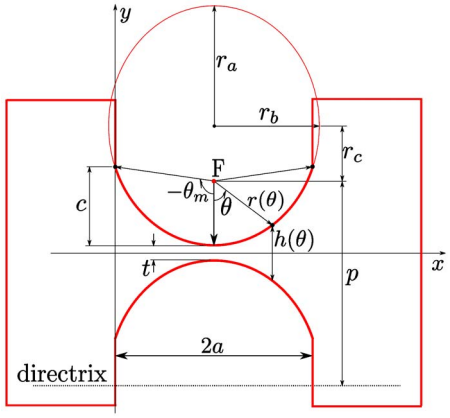

FIG. 3. (Color online) Elliptical arc flexure hinge.

III. CONIC FLEXURE HINGES

A. Elliptical arc flexure hinges

Figure 3 shows an elliptical arc flexure hinge[3] and illustrates the polar coordinates of the upper cutout. It should be noted that $\theta=0$ is always on the major axis, and the generalized conic flexure hinge model does not include the elliptical arc flexure hinges whose major axes are along the cutout length. r_a, r_b are the major and minor semiaxes of the ellipse, respectively. The focal length r_c can be calculated as

$$r_c = \sqrt{r_a^2 - r_b^2}, \tag{5}$$

the eccentricity as

$$e = r_c/r_a, \tag{6}$$

and the distance between one of the foci and the corresponding directrix as

$$p = \frac{r_a^2}{r_c} - r_c = \frac{r_b^2}{r_c}. \tag{7}$$

If the maximum polar angle θ_m of an elliptical arc flexure hinge equals $\pi/2+\arctan(r_c/r_b)$, the cutouts become semiellipses and the hinge becomes an elliptical flexure hinge, which has been discussed in Ref. 2.

As e tends to 0, the hinge converges toward a circular one. At $e=0$, the elliptical arc flexure hinge becomes circular, and we have $p=\infty$ and $r(\theta)=ep=r_a=r_b$. Since it is difficult if not impossible to take the limits of the closed-form solutions presented in the following, a practical way is to approximate the results for circular hinges by using a very small value

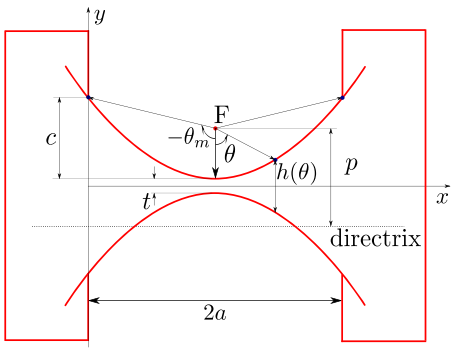

FIG. 4. (Color online) Parabolic flexure hinge.

Author complimentary copy. Redistribution subject to AIP license or copyright, see http://rsi.aip.org/rsi/copyright.jsp

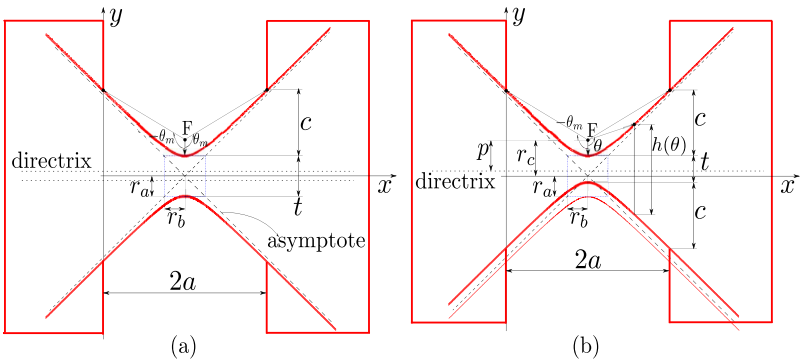

FIG. 5. (Color online) Hyperbolic flexure hinge. (a) The hyperbolic flexure model proposed by Lobontiu *et al.* (Ref. 4), and (b) the extended hyperbolic flexure model.

(e.g., $e=10^{-7}$) to represent $e=0$. The approximate results for a circular hinge are presented and compared with Paros and Weisbord's results[1] in Sec. VI.

B. Parabolic flexure hinges

Figure 4 shows a parabolic flexure hinge and illustrates the polar coordinates of the upper cutout. Due to $e=1$ for a parabola, the distance between its foci and the directrix is given by

$$p = a^2/2c, \tag{8}$$

where $l=2a$ and c are the length and the depth of the parabolic cutout, respectively. The maximum polar angle θ_m can be calculated using Eq. (4).

C. Hyperbolic flexure hinges

Lobontiu *et al.*[4] used three parameters, i.e., the minimum thickness t, the half length of the cutouts a, and the cutout depth c to define the profile of a hyperbolic flexure hinge. In their work, the thickness was given by

$$h(x) = \sqrt{t^2 + 4c(c+t)\left(1 - \frac{x}{a}\right)^2}. \tag{9}$$

Equation (9) indicates that the two symmetric cutouts are located on the same hyperbola, i.e., t must equal $2r_a$ (r_a is the real semiaxis of the hyperbola), as shown in Fig. 5(a). In this paper, we extend this definition by using four parameters (e, p, θ_m, and t) to determine the profile of a hyperbolic flexure hinge, with t an independent variable to the hyperbolic curve, as shown in Fig. 5(b).

Figure 5(b) shows hyperbolic flexure hinges and illustrates the polar coordinates of the upper hyperbolic cutout. For a hyperbola, the distance between one of the foci and the corresponding directrix is given by

$$p = r_c - \frac{r_a^2}{r_c} = \frac{r_b^2}{r_c}, \tag{10}$$

where r_c is the focal length, and r_a and r_b are the semimajor axis (the foci lie on the extension of the major axis of the hyperbola) and the semiminor axis, respectively.

IV. COMPLIANCE EQUATIONS FOR CONIC FLEXURE HINGES

Slice the profile of the hinge region of a conic flexure hinge into vertical infinitesimal strips. The height of the infinitesimal strip $d\theta$ at position θ can be expressed uniformly as

$$h(\theta) = \frac{2ep}{1+e} + t - 2r(\theta)\cos\,\theta. \tag{11}$$

Let $s=p/t$ and

$$q = \frac{2e}{1+e} + \frac{1}{s}, \tag{12}$$

then $h(\theta)$ can be expressed as

$$h(\theta) = p\left(q - \frac{2e\cos\,\theta}{1+e\cos\,\theta}\right) = pg(\theta). \tag{13}$$

The relationship between x and θ can be expressed as

$$x = a + r(\theta)\sin\,\theta. \tag{14}$$

Differentiating Eq. (14) results

$$dx = [r'(\theta)\sin\,\theta + r(\theta)\cos\,\theta]d\theta = \frac{ep(e+\cos\,\theta)}{(1+e\cos\,\theta)^2}d\theta. \tag{15}$$

A. Compliance matrix

It is assumed that the minimum thickness of a flexure hinge t is much smaller than the cutout length l, say $t \leq 0.2l$, so the hinge can be treated as a six degree-of-freedom fixed-free beam subject to bending, axial loading, shearing and torsion, as shown in Fig. 1. By defining the force actuating on the hinge by

$$\mathbf{F} = [F_x, F_y, F_z, M_x, M_y, M_z]^T \tag{16}$$

and the corresponding deformations of the hinge by

$$\mathbf{X} = [\Delta_x, \Delta_y, \Delta_z, \alpha_x, \alpha_y, \alpha_z]^T, \tag{17}$$

the following relationship is obtained:

Author complimentary copy. Redistribution subject to AIP license or copyright, see http://rsi.aip.org/rsi/copyright.jsp

$$\mathbf{X} = \mathbf{C}_h \mathbf{F}, \tag{18}$$

where $\mathbf{C}_h$ is the compliance matrix of the hinge, which can be expressed by

$$\mathbf{C}_h = \begin{Bmatrix} \Delta_x/F_x & 0 & 0 & 0 & 0 & 0 \\ 0 & \Delta_y/F_y & 0 & 0 & 0 & \Delta_y/M_z \\ 0 & 0 & \Delta_z/F_z & 0 & \Delta_z/M_y & 0 \\ 0 & 0 & 0 & \alpha_x/M_x & 0 & 0 \\ 0 & 0 & \alpha_y/F_z & 0 & \alpha_y/M_y & 0 \\ 0 & \alpha_z/F_y & 0 & 0 & 0 & \alpha_z/M_z \end{Bmatrix}. \tag{19}$$

Because the compliance matrix is symmetric,[3] we have $\alpha_z/F_y = \Delta_y/M_z$ and $\alpha_y/F_z = \Delta_z/M_y$. Each element in the compliance matrix is derived from beam theory in the following.

B. Angular compliance about the *z* axis

The z axis is the input axis of a flexure hinge. The angular compliance corresponding to moment M_z can be expressed as

$$\frac{\alpha_z}{M_z} = \int_{-\theta_m}^{\theta_m} \frac{\dfrac{ep(e+\cos\theta)}{(1+e\cos\theta)^2}}{EI_z(\theta)} d\theta = \int_{-\theta_m}^{\theta_m} \frac{ep(e+\cos\theta)}{E[wh^3(\theta)/12](1+e\cos\theta)^2} d\theta = \frac{12e}{Ewp^2} N_1, \tag{20}$$

where E is the elastic modulus of the material, $I_z(\theta)$ is the cross-sectional area moment of inertia about the neutral axis at the given position θ, and

$$N_1 = \int_{-\theta_m}^{\theta_m} \frac{e+\cos\theta}{g^3(\theta)(1+e\cos\theta)^2} d\theta = \frac{q^3 + e^2(2q+5q^2-2q^3) + e^4(q-2)^2(q-1) + e[q^2(q-1) - e^2(8+2q-7q^2+2q^3) + e^4(q-2)^3]\cos\theta_m}{0.5[e^2(q-2)^2 - q^2]^2[q+e(q-2)\cos\theta_m]^2 \csc\theta_m} - \frac{12e[e^2(q-2)-q]\operatorname{arccoth}\dfrac{[q+e(q-2)]\cot(\theta_m/2)}{\sqrt{e^2(q-2)^2-q^2}}}{[e^2(q-2)^2-q^2]^{5/2}}. \tag{21}$$

The contribution of F_y to α_z equals its equivalent moment $F_y[a - ep\sin\theta/(1+e\cos\theta)]$. Therefore, the angular compliance corresponding to force F_y can be calculated as

$$\frac{\alpha_z}{F_y} = \int_{-\theta_m}^{\theta_m} \frac{\left(a - \dfrac{ep\sin\theta}{1+e\cos\theta}\right)\dfrac{ep(e+\cos\theta)}{(1+e\cos\theta)^2}}{E[wh^3(\theta)]/12} d\theta = \int_{-\theta_m}^{\theta_m} \left\{ \frac{aep(e+\cos\theta)}{E[wh^3(\theta)](1+e\cos\theta)^2/12} - \frac{e^2p^2(e+\cos\theta)\sin\theta}{E[wh^3(\theta)](1+e\cos\theta)^3/12} \right\} d\theta = \frac{12ae}{Ewp^2} N_1. \tag{22}$$

C. Angular compliance about the *y* axis

The angular compliance about the y axis corresponding to moment M_y is given by

$$\frac{\alpha_y}{M_y} = \int_{-\theta_m}^{\theta_m} \frac{\dfrac{ep(e+\cos\theta)}{(1+e\cos\theta)^2}}{EI_y(\theta)} d\theta = \frac{12e}{Ew^3} N_2, \tag{23}$$

where

$$N_2 = \int_{-\theta_m}^{\theta_m} \frac{e+\cos\theta}{g(\theta)(1+e\cos\theta)^2} d\theta = \frac{2\sqrt{e^2-1}\,\operatorname{arccoth}\dfrac{(e+1)\cot(\theta_m/2)}{\sqrt{e^2-1}}}{e} + \frac{2[q-e^2(q-2)]\operatorname{arccoth}\dfrac{(q+qe-2e)\cot(\theta_m/2)}{\sqrt{e^2(q-2)^2-q^2}}}{e\sqrt{e^2(q-2)^2-q^2}}. \tag{24}$$

The contribution of F_z to α_y equals its equivalent moment $-F_z[a - ep\sin\theta/(1+e\cos\theta)]$. Thus, the angular compliance corresponding to force F_y is

$$\frac{\alpha_y}{F_z} = \int_{-\theta_m}^{\theta_m} \frac{-\left(a - \dfrac{ep\sin\theta}{1+e\cos\theta}\right)\dfrac{ep(e+\cos\theta)}{(1+e\cos\theta)^2}}{E[w^3h(\theta)]/12} d\theta = -\frac{12ae}{Ew^3} N_2. \tag{25}$$

D. Linear compliance along the *z* axis

Because the compliance matrix is symmetric, the linear compliance along the z axis corresponding to moment M_y is

Author complimentary copy. Redistribution subject to AIP license or copyright, see http://rsi.aip.org/rsi/copyright.jsp

$$\frac{\Delta_z}{M_y} = \frac{\alpha_y}{F_z} = -\frac{12ae}{Ew^3}N_2. \tag{26}$$

The linear compliance along the z axis corresponding to force F_z can be divided into two parts, namely, the bending part (denoted as Δ_z^b/F_z) and the shearing part (denoted as Δ_z^s/F_z). The shearing part can be calculated as

$$\frac{\Delta_z^s}{F_z} = \int_0^{2a} \frac{k}{Gwh(x)}dx = \frac{kep}{Gw}\int_{-\theta_m}^{\theta_m} \frac{e+\cos\theta}{h(\theta)(1+e\cos\theta)^2}d\theta = \frac{ke}{Gw}N_2, \tag{27}$$

where G and k are the shearing modulus and shearing coefficient of the material, respectively. For a beam of rectangular cross section, k is[8]

$$k = \frac{12+11\nu}{10+10\nu}, \tag{28}$$

where ν is Poisson's ratio, and

$$\nu = \frac{E}{2G} - 1. \tag{29}$$

The bending part is

$$\frac{\Delta_z^b}{F_z} = -\int_{-\theta_m}^{\theta_m}\left[\int_{-\theta_m}^{\theta} \frac{-\left(a-\frac{ep\sin\beta}{1+e\cos\beta}\right)\frac{ep(e+\cos\beta)}{(1+e\cos\beta)^2}}{E[w^3h(\beta)/12]}d\beta\right]d\left(\frac{ep\sin\theta}{1+e\cos\theta}\right) = \frac{12a^2e}{Ew^3}N_2 + \frac{12e^3p^2}{Ew^3}N_3, \tag{30}$$

where

$$N_3 = \int_{-\theta_m}^{\theta_m}\frac{\sin^2\theta(e+\cos\theta)}{g(\theta)(1+e\cos\theta)^4}d\theta = \frac{[(q-qe^2+2e^2)^2-2e^2]\operatorname{arccoth}\frac{(1+e)\cot(\theta_m/2)}{\sqrt{e^2-1}}}{2e^3\sqrt{e^2-1}} - \frac{[q^3-2qe^2(2-3q+q^2)+e^4(q-2)^3]\operatorname{arccoth}\frac{(q-2e+qe)\cot(\theta_m/2)}{\sqrt{e^2(q-2)^2-q^2}}}{2e^3\sqrt{e^2(q-2)^2-q^2}} + \frac{q-e^2(q-3)+e(1+q+2e^2-qe^2)\cos\theta_m}{2e^2\csc\theta_m(1+e\cos\theta_m)^2}. \tag{31}$$

To sum up, the linear compliance along the z axis due to F_z is

$$\frac{\Delta_z}{F_z} = \left(\frac{12a^2e}{Ew^3} + \frac{ke}{Gw}\right)N_2 + \frac{12e^3p^2}{Ew^3}N_3. \tag{32}$$

E. Linear compliance along the *y* axis

Again, because the compliance matrix is symmetric, the linear compliance along the y axis corresponding to moment M_z is

$$\frac{\Delta_y}{M_z} = \frac{\alpha_z}{F_y} = \frac{12ae}{Ewp^2}N_1. \tag{33}$$

By following the derivation of Δ_z/M_y, the linear compliance along the y axis corresponding to F_y can be derived as

$$\frac{\Delta_y}{F_y} = \frac{12a^2e}{Ewp^2}N_1 + \frac{12e^3}{Ew}N_4 + \frac{ke}{Gw}N_2, \tag{34}$$

where

$$N_4 = \int_{-\theta_m}^{\theta_m}\frac{\sin^2\theta(e+\cos\theta)}{g^3(\theta)(1+e\cos\theta)^4}d\theta = \frac{(e^2-1)^{3/2}}{2e^3}\operatorname{arctanh}\frac{(e-1)\tan(\theta_m/2)}{\sqrt{e^2-1}} - \frac{[12e^4-8e^6-6q^2e^2(e^2-1)^2+(qe^2-q)^3+6q(e^2-3e^4+2e^6)]\operatorname{arctanh}\frac{(qe-q-2e)\tan(\theta_m/2)}{\sqrt{4e^2-4qe^2+q^2(e^2-1)}}}{2e^3[4e^2-4qe^2+q^2(e^2-1)]^{3/2}} - \frac{4e^4-2qe^2-3q^2e^2(e^2-1)+q^3(e^2-1)^2+e[q^3(e^2-1)^2-8e^2(e^2-1)+2qe^2(6e^2-7)-q^2(6e^4-9e^2+3)]\cos\theta_m}{2e^2\csc\theta_m[4e^2-4qe^2+q^2(e^2-1)][q+e(q-2)\cos(\theta_m/2)]^2}, \tag{35}$$

Author complimentary copy. Redistribution subject to AIP license or copyright, see http://rsi.aip.org/rsi/copyright.jsp

TABLE I. Six design examples of conic flexure hinges. For each of the designs, $w=10$ mm, $a=4$ mm, $c=2$ mm, $t=0.2$ mm, and the material is 45 grade steel (with a Young's modulus of 2.07×10^{11} N/m^2 and a shearing modulus of 8.1×10^{10} N/m^2).

Example	Type	e	p (mm)	θ_m (deg)
1	Circular	10^{-7}	5×10^7	53.13
2	Elliptical arc	0.4	12.1	69.98
3	Elliptical arc	0.7	6.44	80.73
4	Parabolic	1	4.00	90
5	Hyperbolic	1.5	1.83	102.68
6	Hyperbolic	2.2	0.73	115.99

and for parabolic hinges, i.e., $e=1$, we have

$$\lim_{e\to1}\left[\sqrt{e^2\pm1}\ \operatorname{arctanh}\frac{(e-1)\tan(\theta_m/2)}{\sqrt{e^2-1}}\right]=0. \tag{36}$$

F. Linear compliance along the *x* axis

The linear compliance along the x axis can be expressed as

$$\frac{\Delta_x}{F_x}=\int_{-\theta_m}^{\theta_m}\frac{\dfrac{ep(e+\cos\theta)}{(1+e\cos\theta)^2}}{Ewh(\theta)}d\theta=\frac{e}{Ew}N_2. \tag{37}$$

G. Angular compliance about the *x* axis

Because each infinitesimal strip of the hinge can be treated as a constant rectangular cross-sectional beam, according to the approximate torsion equation given in Hearn's book,[9] the angular compliance about the x axis can be expressed as

$$\frac{\alpha_x}{M_x}=\int_{-\theta_m}^{\theta_m}\frac{\dfrac{7w^3h(\theta)+7wh^3(\theta)}{2}\dfrac{ep(e+\cos\theta)}{(1+e\cos\theta)^2}}{Gw^4h^4(\theta)}d\theta$$
$$=\frac{7e}{2Gwp^2}N_1+\frac{7e}{2Gw^3}N_2. \tag{38}$$

V. PRECISION EQUATIONS FOR CONIC FLEXURE HINGES

The offset of the center point of the hinge profile (point Q shown in Fig. 1) is often used to characterize the transmission precision of a flexure hinge for convenience.[10] By defining the offset of Q by

$$\mathbf{H}=[\epsilon_x,\epsilon_y,\epsilon_z]^T, \tag{39}$$

the following relationship can be obtained:

$$\mathbf{H}=\mathbf{P}_h\mathbf{F}, \tag{40}$$

where $\mathbf{P}_h$ is the precision matrix of the hinge, which can be expressed as

$$\mathbf{P}_h=\begin{Bmatrix}\epsilon_x/F_x & 0 & 0 & 0 & 0 & 0\\ 0 & \epsilon_y/F_y & 0 & 0 & \epsilon_y/M_z & 0\\ 0 & 0 & \epsilon_z/F_z & \epsilon_z/M_y & 0 & 0\end{Bmatrix}. \tag{41}$$

Each element in the precision matrix is called a precision factor.

A. Precision factor along the *x* axis

The precision factor along the x axis can be calculated as

$$\frac{\epsilon_x}{F_x}=\frac{e}{2Ew}N_2. \tag{42}$$

B. Precision factors along the *y* axis

The precision factor along the y axis corresponding to moment M_z can be expressed as

$$\frac{\epsilon_y}{M_z}=\left[\frac{ep\sin\theta}{1+e\cos\theta}\int_{-\theta_m}^{\theta}\frac{ep(e+\cos\beta)}{Ewh^3(\beta)(1+e\cos\beta)^2/12}d\beta\right]_{-\theta_m}^{0}$$
$$-\int_{-\theta_m}^{0}\frac{12e^2p^2\sin\theta(e+\cos\theta)}{Ewh^3(\theta)(1+e\cos\theta)^3}d\theta=\frac{12e^2}{Ewp}N_5, \tag{43}$$

and the precision factor corresponding to force F_y as

$$\frac{\epsilon_y}{F_y}=\left[\frac{ep\sin\theta}{1+e\cos\theta}\int_{-\theta_m}^{\theta}\frac{\left(a-\dfrac{ep\sin\beta}{1+e\cos\beta}\right)\dfrac{ep(e+\cos\beta)}{(1+e\cos\beta)^2}}{Ewh^3(\beta)/12}d\beta\right]_{-\theta_m}^{0}$$
$$-\int_{-\theta_m}^{0}\frac{ae^2p^2\sin\theta(e+\cos\theta)}{Ewh^3(\theta)(1+e\cos\theta)^3/12}d\theta$$
$$+\int_{-\theta_m}^{0}\frac{e^3p^3\sin^2\theta(e+\cos\theta)}{Ewh^3(\theta)(1+e\cos\theta)^4/12}d\theta$$
$$+\frac{kep}{Gw}\int_{-\theta_m}^{0}\frac{e+\cos\theta}{h(\theta)(1+e\cos\theta)^2}d\theta=\frac{12ae^2}{Ewp}N_5+\frac{6e^3}{Ew}N_4$$
$$+\frac{ke}{2Gw}N_2, \tag{44}$$

where

$$N_5=\int_0^{\theta_m}\frac{\sin\theta(e+\cos\theta)}{g^3(\theta)(1+e\cos\theta)^3}d\theta$$
$$=\frac{q-2e^2+qe^2+2e(q-2)\cos\theta_m}{2e^2(q-2)^2[q+e(q-2)\cos\theta_m]^2}$$
$$-\frac{q(1+e)^2-2e(2+e)}{2e^2(q-2)^2(q-2e+qe)^2}. \tag{45}$$

C. Precision factors along the *z* axis

The precision factor along the z axis corresponding to moment M_y is given by

Author complimentary copy. Redistribution subject to AIP license or copyright, see http://rsi.aip.org/rsi/copyright.jsp

TABLE II. Comparison of compliance factors between finite element results (denoted by *F*) and theoretical results (denoted by *C*). The Paros and Weisbord's results are denoted by *P*.

Example	α_z/M_z (rad/N m)	α_y/M_y ($\times 10^{-4}$ rad/N m)	Δ_z/M_y ($\times 10^{-6}$ 1/N)	Δ_z/F_z ($\times 10^{-8}$ m/N)	Δ_y/M_z (1/N)	Δ_y/F_y (m/N)	Δ_x/F_x ($\times 10^{-9}$ m/N)
1(C)	0.849	7.549	−3.019	3.246	3.397×10^{-3}	1.387×10^{-5}	6.291
1(P)	0.849	7.549	3.019	2.959	3.397×10^{-3}	1.376×10^{-5}	6.291
1(F)	0.859	7.668	−3.117	3.505	3.440×10^{-3}	1.405×10^{-5}	6.517
2(C)	0.836	7.465	−2.986	3.209	3.345×10^{-3}	1.365×10^{-5}	6.421
2(F)	0.846	7.591	−3.084	3.484	3.386×10^{-3}	1.383×10^{-5}	7.021
3(C)	0.808	7.288	−2.915	3.132	3.234×10^{-3}	1.319×10^{-5}	6.074
3(F)	0.822	7.417	−3.013	3.494	3.289×10^{-3}	1.341×10^{-5}	6.322
4(C)	0.763	7.004	−2.802	3.008	3.054×10^{-3}	1.243×10^{-5}	5.837
4(F)	0.775	7.135	−2.899	3.354	3.100×10^{-3}	1.263×10^{-5}	6.063
5(C)	0.640	6.234	−2.493	2.675	2.560×10^{-3}	1.038×10^{-5}	5.195
5(F)	0.646	6.368	−2.589	2.968	2.608×10^{-3}	1.058×10^{-5}	5.451
6(C)	0.216	3.833	−1.533	1.661	8.630×10^{-4}	3.484×10^{-6}	3.194
6(F)	0.230	3.990	−1.634	1.816	9.574×10^{-4}	3.843×10^{-6}	3.558

$$\frac{\epsilon_z}{M_y} = -\left[\frac{ep\sin\theta}{1+e\cos\theta}\int_{-\theta_m}^{\theta}\frac{ep(e+\cos\beta)}{Ew^3h(\beta)(1+e\cos\beta)^2/12}d\beta\right]_{-\theta_m}^{0} + \int_{-\theta_m}^{0}\frac{12e^2p^2\sin\theta(e+\cos\theta)}{Ew^3h(\theta)(1+e\cos\theta)^3}d\theta = -\frac{12e^2p}{Ew^3}N_6, \tag{46}$$

the precision factor corresponding to force F_z by

$$\frac{\epsilon_z}{F_z} = \left[\frac{ep\sin\theta}{1+e\cos\theta}\int_{-\theta_m}^{\theta}\frac{\left(a-\frac{ep\sin\beta}{1+e\cos\beta}\right)\frac{ep(e+\cos\beta)}{(1+e\cos\beta)^2}}{Ew^3h(\beta)/12}d\beta\right]_{-\theta_m}^{0} - \int_{-\theta_m}^{0}\frac{ae^2p^2\sin\theta(e+\cos\theta)}{Ew^3h(\theta)(1+e\cos\theta)^3/12}d\theta + \int_{-\theta_m}^{0}\frac{e^3p^3\sin^2\theta(e+\cos\theta)}{Ew^3h(\theta)(1+e\cos\theta)^4/12}d\theta + \frac{kep}{Gw}\int_{-\theta_m}^{0}\frac{e+\cos\theta}{h(\theta)(1+e\cos\theta)^2}d\theta = \frac{12ae^2p}{Ew^3}N_6 + \frac{6e^3p^2}{Ew^3}N_3 + \frac{ke}{2Gw}N_2, \tag{47}$$

where

$$N_6 = \int_0^{\theta_m}\frac{\sin\theta(e+\cos\theta)}{g(\theta)(1+e\cos\theta)^3}d\theta = \frac{1}{4e^2}\left\{\frac{2e^2-2}{1+e\cos\theta_m} + (q+2e^2-qe^2)\{\log[q+e(q-2)\cos\theta_m] - \log(1+e\cos\theta_m)\}\right\} - \frac{1}{4e^2}\{2e-2+(q+2e^2-qe^2)[\log(q-2e+qe) - \log(1+e)]\}. \tag{48}$$

VI. VERIFICATION OF THE CLOSED-FORM EQUATIONS

A. Finite element verification

Table I lists the physical parameters and geometric parameters of six conic flexure hinge designs. All the hinge designs have the same length ($l=2a=8$ mm), cutout depth ($c=2$ mm) and minimum thickness ($t=0.2$ mm) for comparison purposes. The analytical results listed in Tables II and III were calculated by programming the closed-form equations derived above in MATHEMATICA 6.0. The extended-precision computation and numerical-precision tracking technologies implemented in MATHEMATICA facilitate any

TABLE III. Comparison of precision factors between finite element results (denoted by *F*) and theoretical results (denoted by *C*).

Example	ϵ_x/F_x ($\times 10^{-9}$ m/N)	ϵ_y/M_z (1/N)	ϵ_y/F_y (m/N)	ϵ_z/M_y ($\times 10^{-7}$ 1/N)	ϵ_z/F_z (m/N)
1(C)	3.145	1.775×10^{-4}	8.525×10^{-7}	−3.921	1.176×10^{-8}
1(F)	3.262	1.810×10^{-4}	8.710×10^{-7}	−4.348	1.121×10^{-8}
2(C)	3.110	1.722×10^{-4}	8.258×10^{-7}	−3.858	1.162×10^{-8}
2(F)	3.232	1.759×10^{-4}	8.453×10^{-7}	−4.285	1.108×10^{-8}
3(C)	3.037	1.614×10^{-4}	7.711×10^{-7}	−3.729	1.132×10^{-8}
3(F)	3.161	1.654×10^{-4}	7.920×10^{-7}	−4.051	1.078×10^{-8}
4(C)	2.918	1.446×10^{-4}	6.872×10^{-7}	−3.530	1.085×10^{-8}
4(F)	3.048	1.481×10^{-4}	7.052×10^{-7}	−3.843	1.033×10^{-8}
5(C)	2.597	1.035×10^{-4}	4.855×10^{-7}	−3.041	9.602×10^{-9}
5(F)	2.738	1.062×10^{-4}	4.991×10^{-7}	−3.335	9.244×10^{-9}
6(C)	1.597	1.840×10^{-5}	8.962×10^{-8}	−2.028	6.051×10^{-9}
6(F)	1.783	1.952×10^{-5}	9.464×10^{-8}	−2.221	6.132×10^{-9}

Author complimentary copy. Redistribution subject to AIP license or copyright, see http://rsi.aip.org/rsi/copyright.jsp

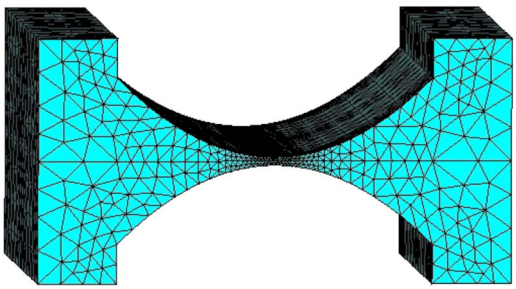

FIG. 6. (Color online) Finite element model.

precision or number size across all functions and guarantee high-precision numerical computations. It can be seen from the analytical results that as e is increased, the hinge becomes less compliant (the compliance factors become smaller), but more accurate (the precision factors become smaller as well).

The finite element software ANSYS was used to check the generalized compliance and precision equations. The finite element models of the designs were generated using Solid72 elements. Solid72 is a four-node element with six degrees of freedom at each node, and is well suited to model irregular shapes and curved boundaries without much loss of accuracy. Each hinge model is fixed at one end, and loaded at the other end. The smart meshing method, which automatically refines meshes in higher stress concentration regions, was used. In order to find out how the mesh influences the accuracy of the solution, several models of example 4 with different levels of mesh refinement were solved for α_z/M_z, in which a model with approximately 65 000 elements was assumed to produce the "exact" solution. By comparing the results, it has been found that the errors of finite element modeling are within 1% when there are four (corresponds to a mesh of approximately 5000 elements) or more elements generated across the thinnest part of the notch region. If the smart meshing generated less than four elements across the thinnest part of the notch region, we refined the local mesh manually to ensure the accuracy of finite element modeling. Figure 6 shows one of the hinge models.

Because the compliance matrix is symmetric, only Δ_x/F_x, Δ_y/F_y, Δ_z/F_z, α_y/M_y, α_z/M_z, Δ_y/M_z, and Δ_z/M_y in the compliance matrix were verified. The analytical and finite element results in Tables II and III are in good agreement. The errors between the analytical and finite element results are less than 11%. For the elliptical arc flexure hinges, these compliance equations have the same results as the ones developed by Chen *et al.*[3] It should be noted that the compliance results for the circular hinge (example 1) were calculated approximately by using $e=10^{-7}$ to represent $e=0$. Also, the corresponding results using the full theoretical equations derived by Paros and Weisbord[1] are presented. Paros and Weisbord's results accord very well with the approximate ones, except Δ_y/F_y and Δ_z/F_z, because we take shearing coefficient k into consideration. The approximate results for Δ_y/F_y and Δ_z/F_z (with the shearing coefficient considered) are more accurate compared to the finite element results.

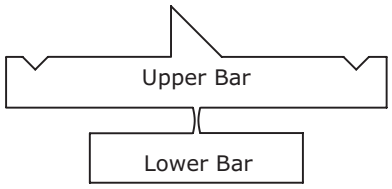

FIG. 7. Diagram of a sample profile.

B. Experimental verification

Experimentation was used to assess the validity of the angular compliance equation about the input axis α_z/M_z. Four conic flexure hinge samples made of 45 grade steel were machined by using Charmilles Robofil 2050TW WEDM machine, which has a profile error less than 1.5 μm. The geometric parameters are listed in Table IV. Each hinge was machined as an "I-shaped" sample with the upper and lower horizontal bars being separated by the hinge itself, a 45° wedge on the upper bar exactly above the hinge, and a triangular cutout on each side of the upper bar, as shown in Fig. 7.

The experimental setup comprises an optical platform, a 6500 A laser diode, a reflector (mounted on the wedge), a position sensitive detector (HAMAMATSU S1880), and a hinge sample, as shown in Fig. 8. The lower bar of the hinge sample, and the position sensitive detector are mounted on the optical platform to be rigidly held in place. The diode laser is fixed immediately above the reflector. A laser beam, which is deflected from the reflector, is directed to the position sensitive detector for measuring the position of the laser spot. The position sensitive detector has a resolution of 1.5 μm over a measuring range of 12 mm. A bandpass filter having 10 nm bandwidth at a center wavelength of 6500 A is attached to the position sensitive detector to suppress ambient light. To improve the measurement precision, the distance between the position sensitive detector and the tested

TABLE IV. Comparison of compliance factor α_z/M_z between experimental results (denoted by X) and theoretical results (denoted by C). For each sample, $w=10$ mm.

Sample	Type	θ_m (deg)	t (mm)	e	p (mm)	X (rad/N m)	C (rad/N m)	% error
1	Parabolic	43.6	0.2	1	5	0.863	0.848	−1.77
2	Hyperbolic	90	0.4	4	0.5	0.109	0.115	5.22
3	Elliptical arc	100	0.2	0.66	3.4	0.592	0.569	−4.04
4	Circular	60	1	10^{-7}	5.774×10^{7}	0.016	0.0152	−5.26

Author complimentary copy. Redistribution subject to AIP license or copyright, see http://rsi.aip.org/rsi/copyright.jsp

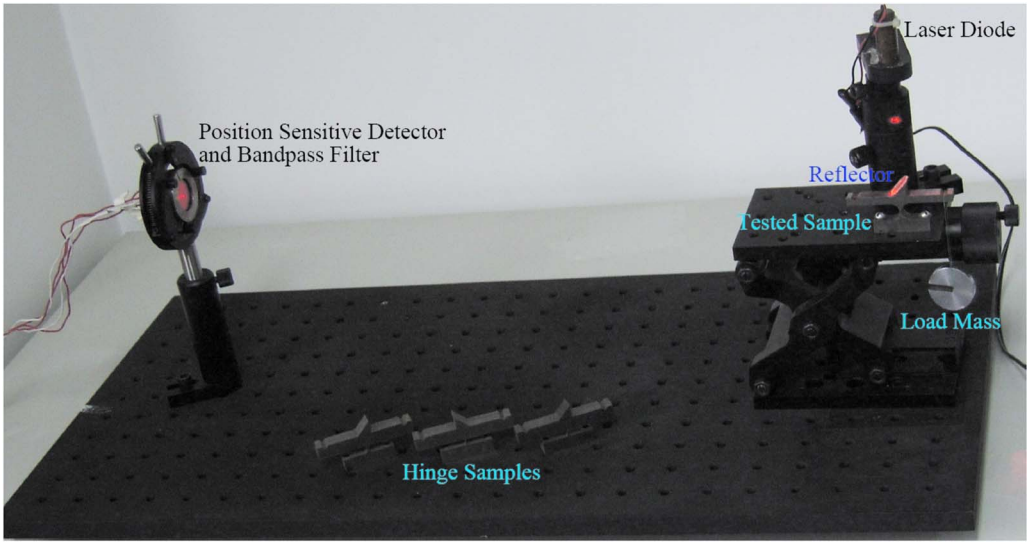

FIG. 8. (Color online) The experimental setup.

hinge should be as long as possible. In the experiments, the position sensitive detector is 500 mm away from the hinges.

As discussed in Ref. 2, there are two major error sources of the experimental results, the uncertainty of the elastic modulus of the hinge material and the machining error of the minimum thickness of the hinge sample. The elastic modulus 45 grade steel is estimated to range from 2×10^{11} to 2.1×10^{11} N/m^2 and therefore using 2.07×10^{11} N/m^2 as the elastic modulus may result in an error less than 3.5%. A digital vernier caliper with a resolution of 5 μm was used to measure the minimum thickness of each sample. The measured results are within an error of 10 μm compared to the corresponding design values. This gives an error no more than 5% for the thinnest hinge sample of thickness 0.2 mm. Moreover, it should be noted that the reflected laser beam doubles the angular deflection of the sample, which improves the measuring precision by reducing the percentage errors due to hinge compression and parasitic deflections. Therefore, a worst case error of $\pm$8.5% can be a reasonable estimate for the experimental results.

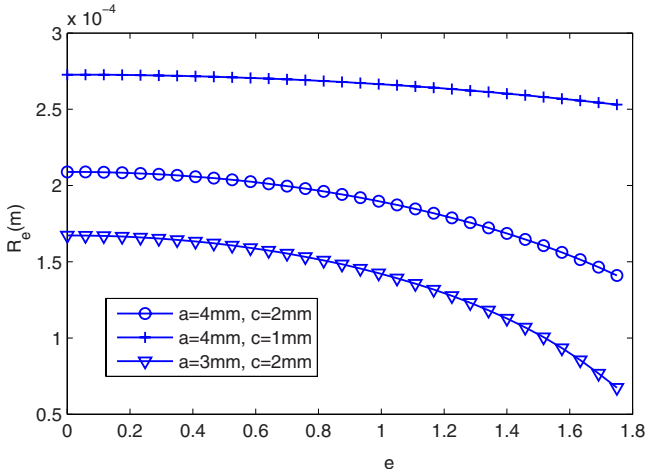

FIG. 9. (Color online) The relative errors of conic hinges as a function of eccentricity e for different (a,c) pairs. The other parameters used in calculation are $w=10$ mm, $t=0.2$ mm, and $E=2.07\times10^{11}$ N/m^2.

For each sample, we loaded a mass of 50 g at both triangular cutouts (force arm of 25 mm) to simulate two bending load cases, so two compliance values were obtained. The corresponding angular compliance was calculated as an average. When the hinge sample deformed due to the load, the position sensitive detector read the displacement of the laser spot on itself, which was used to calculate the angular deflection of the sample. The experimental results are summarized in Table IV. The results are within 6% error compared to the analytical results.

VII. A CASE STUDY

When determining optimal hinge designs for a flexure-based mechanism, it is necessary to consider the design specification in terms of the accuracy, load capability, displacement range, allowable hinge volume, and other application specific constraints.[2] A full-scale discussion on this is beyond the scope of this paper. Nevertheless, we present a case study to demonstrate the use of the generalized model in selecting hinge profiles.

There are many applications where accuracy is the most important factor while other factors are less important, such as optical disk systems[5] and nanopositioning stages.[11] In these applications, circular flexure hinges are always chosen[5,11] because it has been widely accepted that circular flexure hinges are more accurate than other types of hinge. It can be seen from Table III, however, that the circular hinge has the largest precision factors, which indicates that circular hinges produce more parasitic deflection than the others in the conic family of flexure hinges when subject to the same load. Because designs often require a specified angular displacement,[2] it is necessary and appropriate to compare the accuracy of different hinges on the basis of a given angular displacement. We assume that a pure moment M_z is applied, and we define the ratio of precision factor ϵ_y/M_z and compliance factor α_z/M_z as a new term "relative error:"

Author complimentary copy. Redistribution subject to AIP license or copyright, see http://rsi.aip.org/rsi/copyright.jsp

$$R_e = \frac{\epsilon_y / M_z}{\alpha_z / M_z} = \frac{epN_5}{N_1}. \quad (49)$$

A hinge with a smaller relative error produces less parasitic motion when outputting the same angular deflection about the z axis, and is thus more accurate. Figure 9 plots the relative errors of conic hinges as a function of eccentricity e. Each curve in Fig. 9 is plotted with equal E, w, a, c, and t, which ensures that different kinds of flexure hinge are compared on an equal basis. We can see from Fig. 9 that in the conic family of flexure hinges, the hyperbolic ones ($e>1$) are the most precise, while circular ones ($e=0$) are the least precise.

ACKNOWLEDGMENTS

The authors would like to thank the editors and the reviewers for their valuable and insightful comments. This research was supported by the National Natural Science Foundation of China under Grant No. 50805110, the Key Project of Chinese Ministry of Education under Grant No. 109145, and the China Postdoctoral Science Foundation under Grant No. 20070421110.

[1] J. M. Paros and L. Weisbord, Mach. Des. **37**, 151 (1965).
[2] S. T. Smith, V. G. Badami, J. S. Dale, and Y. Xu, Rev. Sci. Instrum. **68**, 1474 (1997).
[3] G. M. Chen, X. D. Shao, and X. B. Huang, Rev. Sci. Instrum. **79**, 095103 (2008).
[4] N. Lobontiu, J. S. N. Paine, E. Garcia, and M. Goldfarb, Mech. Mach. Theory **37**, 477 (2002).
[5] C. S. Han and S. H. Kim, Rev. Sci. Instrum. **73**, 3678 (2002).
[6] J. H. Kim, S. H. Kim, and Y. K. Kwak, Sens. Actuators, A **116**, 530 (2004).
[7] J. W. Ryu, S. Q. Lee, D. G. Gweon, and K. S. Moon, Mechatronics **9**, 657 (1999).
[8] S. P. Timoshenko and J. M. Gere, *Mechanics of Materials* (Van Nostrand Reinhold, New York, 1972).
[9] E. J. Hearn, *Mechanics of Materials: An Introduction to the Mechanics of Elastic and Plastic Deformation of Solids and Structural* (Pergamon, Oxford, 1977).
[10] L. L. Howell, *Compliant Mechanisms* (Wiley, New York, 2001).
[11] Y. K. Yong, S. S. Aphale, and S. O. R. Moheimani, IEEE Trans. Nanotechnol. **8**, 46 (2009).

Author complimentary copy. Redistribution subject to AIP license or copyright, see http://rsi.aip.org/rsi/copyright.jsp